Chemistry Europe
European Chemical
Societies Publishing

WILEY-VCH

Excellence in Chemistry Research

Announcing
our new
flagship journal

- Gold Open Access
- Publishing charges waived
- Preprints welcome
- Edited by active scientists

Chemistry
Europe

Excellence in Chemistry Research Worldwide

Front Cover:
Photo by Rodion Kutsaiev on Unsplash

journal.chemistry-europe.org

WILEY-VCH

Meet the Editors of *ChemistryEurope*

**Luisa De Cola**
Università degli Studi
di Milano Statale, Italy

**Ive Hermans**
University of
Wisconsin-Madison, USA

**Ken Tanaka**
Tokyo Institute of
Technology, Japan

ChemPubSoc Europe

DOI: 10.1002/cctc.201801976

CHEMCATCHEM
Full Papers

# Synthesis of Nickel-Doped Ceria Catalysts for Selective Acetylene Hydrogenation

Christopher Riley,[a] Andrew De La Riva,[a] Shulan Zhou,[b, c] Qiang Wan,[d] Eric Peterson,[a] Kateryna Artyushkova,[a] Majid D. Farahani,[e] Holger B. Friedrich,[e] Laura Burkemper,[f] Nicu-Viorel Atudorei,[f] Sen Lin,[d] Hua Guo,[b] and Abhaya Datye*[a]

Metallic nickel is known to be an active, but not a selective hydrogenation catalyst for conversion of alkynes to alkenes. On the other hand, nickel oxide is not active. Recently, we have demonstrated that nickel doped into ceria provides an inexpensive catalyst for selective hydrogenation of acetylene in the presence of ethylene. Here, we evaluate various synthesis methods to achieve optimal selective hydrogenation performance. We examined incipient wetness impregnation, coprecipitation, solution combustion, and sol-gel synthesis to study how the method of preparation affects catalytic structure and behavior. Sol-gel synthesis, coprecipitation, and solution combustion synthesis methods favor nickel incorporation into the ceria lattice, while incipient wetness impregnation creates segregated nickel species on the ceria surface. For hydrogenation of acetylene, these nickel surface species lead to poor ethylene selectivity due to ethane and oligomer formation. However, when nickel is incorporated into the ceria lattice, ethane formation is prevented even while achieving 100% conversion of acetylene. Coke formation is also significantly reduced on these catalysts compared to conventional nanoparticle counterparts. We conclude that sol-gel synthesis provides the optimal method for creating a uniform dopant distribution within the high surface area ceria.

## Introduction

Recent work has shown that ceria ($CeO_2$) catalyzes the semi-hydrogenation of acetylene,[1–4] which is a chemical reaction used to purify ethylene streams. In an unmodified form, however, $CeO_2$ has a low hydrogenation activity and requires high operation temperature.[4] Our recent work suggested oxygen vacancies as the active hydrogenation sites.[5] These sites are present on ceria surfaces as defects in relatively low concentrations. However, the oxygen vacancy concentration can be increased with the incorporation of nickel dopants into the ceria lattice.[5] The substitution of cerium ions by nickel ions creates a charge imbalance, which is compensated by the removal of an oxygen ion from the ceria surface.[6] Nickel-doped ceria surfaces, having higher concentrations of active vacancy sites, show dramatically higher activity than ceria alone. In this work, we analyze various synthesis techniques for producing doped nickel-ceria and study the hydrogenation behavior of the resulting catalysts.

Activity is not the only consideration when designing an effective acetylene hydrogenation catalyst; the catalyst must also be selective towards ethylene. Traditional palladium-based catalysts are not selective for acetylene hydrogenation, as metallic palladium over-hydrogenates ethylene to ethane.[7] Metallic nickel represents a promising alternative to palladium catalysts because it is much less expensive. While nickel is active for hydrogenation, this metal oligomerizes hydrocarbon reactants, which substantially reduces ethylene selectivity.[8,9] Ethylene selectivity of both metals is improved through alloying with inactive metals to form bimetallic particles.[7,10–13] By dispersing active metal sites, the geometric, chemical, and electronic properties of the catalyst are adjusted in favor of ethylene production.[7,14] Nonetheless, bimetallic particles still produce ethane and oligomers.[10–13,15] The use of gold, and other precious metals, as the alloying element further increases catalyst cost.[15–19]

Nickel-doped ceria may serve as a cheap and selective alternative catalyst for several reasons. First, nickel dopants incorporated into the ceria lattice are in an oxidized state and are not readily reduced, in contrast to nickel surface species.[5] Rodríguez et al. indicated the need for three neighboring Ni

---

[a] C. Riley, Dr. A. De La Riva, Dr. E. Peterson, Dr. K. Artyushkova, Prof. A. Datye
Department of Chemical and Biological Engineering and Center for Micro-engineered Materials
University of New Mexico
Albuquerque, New Mexico 87131 (USA)
E-mail: datye@unm.edu
[b] Dr. S. Zhou, Prof. H. Guo
Department of Chemistry and Chemical Biology
University of New Mexico
Albuquerque, New Mexico 87131 (USA)
[c] Dr. S. Zhou
Department of Material Science and Engineering
Jingdezhen Ceramic Institute
Jingdezhen 333403 (China)
[d] Q. Wan, Prof. S. Lin
State Key Laboratory of Photocatalysis on Energy and Environment
Fuzhou University
Fuzhou 350002 (China)
[e] Dr. M. D. Farahani, Prof. H. B. Friedrich
Catalysis Research Group, School of Chemistry and Physics
Westville Campus, University of KwaZulu-Natal
Durban 4000 (South Africa)
[f] Dr. L. Burkemper, Dr. N.-V. Atudorei
Center for Stable Isotopes
University of New Mexico
Albuquerque, New Mexico, 87131 (USA)

Supporting information for this article is available on the WWW under https://doi.org/10.1002/cctc.201801976

© 2019 Wiley-VCH Verlag GmbH & Co. KGaA, Weinheim

atoms to oligomerize acetylene,[11] so a metal cluster is required. Thus, oligomer production is expected to decrease on doped Ni as a result, compared to metallic nickel counterparts. Second, oxygen vacancy sites offer a different hydrogenation mechanism than metal surfaces.[5] Nickel-doped ceria has been studied in many different reactions, including methane reforming,[20,21] CO oxidation,[22] and hydrogenation of CO, benzene, and ketones.[23,24] To the best of our knowledge, there is no in-depth study of the activity and selectivity of nickel-doped ceria for acetylene semi-hydrogenation, except for our recent work.[5]

Multiple experimental studies have investigated incorporation of nickel into ceria.[25–31] As reported, nickel precursor,[32] loading,[25,27,33] and synthesis technique[34] determine the type of nickel species in the final catalyst. Detected nickel species can consist of large NiO particles on the ceria surface, small NiO ensembles on the ceria surface with enhanced phase interaction, and nickel ions incorporated into the ceria crystal lattice.[28] Incorporation of nickel ions into the ceria lattice may be determined through the absence of x-ray diffraction (XRD) NiO peaks and a decrease in ceria lattice constant (due to the smaller ionic radius of nickel compared to that of cerium).[28] Further, the shifting of nickel peaks to higher binding energy in x-ray photoelectron spectroscopy (XPS) spectra can signal the formation of nickel-ceria solid solutions.[25,26] While TEM-EDX mapping is traditionally used to study the composition and structure of catalysts, it is less useful here due to the strongly absorbing nature of the ceria support. As we demonstrate in the supporting information, XRD and XPS are more effective at detecting segregation of Ni species. This is shown through changes in $CeO_2$ lattice constant and through clear distinction of peaks corresponding to Ni doped into the lattice and Ni present on the $CeO_2$ surface.

This paper aims to evaluate various techniques for synthesis of Ni-doped ceria catalysts and find the one that produces the most active nickel-ceria structure without sacrificing ethylene selectivity. Four synthesis techniques were investigated, which allowed different levels of interaction between nickel and cerium precursors. Nickel was deposited onto ceria via incipient wetness impregnation, representing minimal precursor interaction. In contrast, the cerium precursor was intimately mixed with nickel during coprecipitation, sol-gel, and solution combustion syntheses. Nickel loading was kept low to discourage the formation of a nickel oxide phase. Our results show that segregated nickel phases lead to poor selectivity, while nickel incorporated into the lattice of ceria is selective, preventing the formation of ethane. Therefore, acetylene hydrogenation serves as a sensitive probe to characterize the nature of nickel species in these catalysts.

## Materials and Methods

Ni–$CeO_2$ catalysts were synthesized through incipient wetness impregnation (WI), coprecipitation (CP), sol-gel (SG) and solution combustion synthesis (SCS) techniques. These techniques were chosen to vary the extent and nature of interaction between nickel and cerium precursors during synthesis. The resulting 1.5 wt% Ni–$CeO_2$ samples are herein referred to as 1.5-WI, 1.5-CP, 1.5-SG and 1.5-SCS, respectively. As a reference for nickel nanoparticle characterization and performance, 10 wt% Ni–$SiO_2$ (10-$SiO_2$) was synthesized via wet impregnation of nickel nitrate solution onto silica gel (Aldrich, Davisil grade 643), followed by calcination. Lindlar catalyst (TCI America), was used as a reference sample to represent an industrially used acetylene hydrogenation catalyst, which consists of 5 wt% Pd on calcium carbonate poisoned with lead. This sample is labeled as Lindlar. Additionally, a pure ceria ($CeO_2$) sample was made via calcination of cerium nitrate. Cerium (III) nitrate hexahydrate (Aldrich, 99% trace metals basis) and nickel (II) nitrate hexahydrate (Alfa Aesar, 99.9985% metals basis) were used in each nickel-ceria synthesis except for 1.5-SCS (see below). 1.5-WI samples were synthesized by adding nickel nitrate solution dropwise to ceria that had been calcined at 500 °C. The resulting material was dried at 110 °C overnight and then calcined. 1.5-CP samples were made by first dissolving appropriate amounts of nickel and cerium precursor in 100 ml DI water while stirring. A 1 M solution of potassium hydroxide (EDM Millipore) was prepared. KOH solution was then added dropwise to bring the pH to 10. Additional KOH was added over the next hour to maintain pH $>9$. Stirring was then stopped to allow cerium and nickel hydroxide precipitate to settle overnight. The precipitate was then repeatedly washed with DI water. The resulting precipitate was dried at 110 °C overnight and then calcined. Sol-gel synthesis was performed by dissolving 5 g of polyvinylpyrrolidone (Aldrich 40,000 average molecular weight) into 100 ml of DI water under vigorous stirring and mild heating. The solution was cooled and appropriate amounts of nickel and cerium nitrates were added. This solution was stirred for 1 hour and then dried at 90 °C in a box furnace to form a hard gel. The resulting gel was coarsely ground and calcined. Solution combustion synthesis was conducted by adding ammonium cerium (IV) nitrate (Aldrich, ACS reagent $\geq$98.5%), nickel (II) nitrate hexahydrate, and urea (VWR, high purity) to DI water. The mixture was stirred and heated for approximately half an hour to evaporate excess water. The resulting gel was placed into a furnace at 400 °C to combust. Following combustion, the sample was ground and calcined at 400 °C for 4 hours. All other sample calcinations were performed at 500 °C for 2 hours. Metallic nickel ($Ni^0$) and nickel oxide (NiO) references were synthesized for XPS analysis. NiO was synthesized by calcining nickel (II) nitrate hexahydrate. An aliquot of this material was then reduced in hydrogen for 1 hour at 500 °C, cooled to room temperature, and passivated in air. This treatment formed $Ni^0$ with a surface layer of NiO which could be removed through sputtering.

Samples were characterized using electron probe microanalysis (EPMA), Brunauer-Emmett-Teller (BET) analysis, x-ray diffraction (XRD), x-ray photoelectron spectroscopy (XPS), transmission electron microscopy (TEM), and carbon compositional analysis. EPMA was used to measure bulk elemental composition with a JEOL JXA-8200 Superprobe WD/ED combined microanalyzer. BET analysis was performed using a Micromeritics Gemini 2360 Surface Area Analyzer with liquid nitrogen coolant. XRD analysis was conducted using a Rigaku SmartLab

© 2019 Wiley-VCH Verlag GmbH & Co. KGaA, Weinheim

18673899, 2019, 5, Downloaded from https://chemistry-europe.onlinelibrary.wiley.com/doi/10.1002/cctc.201801976 by Purdue University (West Lafayette), Wiley Online Library on [11/07/2023]. See the Terms and Conditions (https://onlinelibrary.wiley.com/terms-and-conditions) on Wiley Online Library for rules of use; OA articles are governed by the applicable Creative Commons License

diffractometer with a D/TeX detector and copper $K_\alpha$ radiation. Samples were outgassed at 120 °C in flowing nitrogen overnight prior to BET analysis. A 0.02° step size was used with a scan rate of 6.2° min$^{-1}$. To determine accurate lattice parameters, a corundum standard was mixed with select Ni–$CeO_2$ samples. Patterns without the standard are shown in Figure 1. XPS was used to identify the nickel species in 1.5-CP and 1.5-WI samples after reaction. Metallic nickel ($Ni^0$) and nickel oxide (NiO) references were also analyzed. A Kratos AXIS DLD Ultra photoelectron spectrometer was used to gather spectra. The spectrometer had a monochromatic Al $K_\alpha$ source operating at 225 W. Charge compensation was accomplished using low energy electrons. Survey spectra were completed first at 80 eV pass energy for 3 minutes. High-resolution C 1s, O 1s, Ce 3d and Ni 2p spectra were then acquired at pass energy of 20 eV. Quantitative analysis was done in CASAxps. All spectra were charge referenced to aliphatic carbon at 285.0 eV. Curve fitting analysis was carried out using individual peaks of constrained width, position, and shape (70 % Gaussian and 30 % Lorentzian). TEM analysis was conducted using a JEOL JEM 2010F field emission microscope in high angle annular dark field (HAADF) imaging and EDS mapping modes. Carbon compositional analysis was performed to obtain carbon composition as wt % in select catalyst samples before and after reaction. The analysis was conducted using a Costech ECS 4010 Elemental Analyzer coupled to a ThermoFisher Scientific Delta V Plus mass spectrometer via a Conflo IV interface. The elemental analyzer combusts the samples at 980 °C and isolates carbon dioxide through GC separation before sending the gaseous sample to the mass spectrometer for detection. The amount of carbon in the sample is related to the amount of carbon dioxide detected.

Prior to catalytic testing, each sample was sieved between No. 140 and No. 60 sieves, and the particles 105–250 microns in diameter were used for acetylene hydrogenation reaction. First, competitive hydrogenation reactions were performed with both acetylene and ethylene in the feed gas to mimic industrial conditions. Light-off curves were developed under this condition, and catalyst tendency toward over-hydrogenation in the presence of excess ethylene was measured. For these tests, 200 mg of sieved $CeO_2$ and Ni–$CeO_2$ samples and 30 mg of Lindlar catalyst were loaded into a 1/8 inch I.D. glass tube reactor and held in place with glass wool plugs. The samples were oxidized in flowing air (48 ml/min) and then cooled while flushing with nitrogen. Samples were subsequently reduced in flowing hydrogen (2 ml/min) and nitrogen (48 ml/min) and then cooled while flushing with nitrogen. Both oxidation and reduction were performed at 350 °C for 1 hour. The 10-$SiO_2$ sample received a different heat treatment during catalytic testing. The heat treatment involved prereduction in a tube furnace at 600 °C for 4 hours in 7 % hydrogen (balance nitrogen) with a 50 ml/min flow rate. The sample was then cooled to room temperature in flowing hydrogen. Prior to reaction, the 10-$SiO_2$ sample was not oxidized on stream as were the other samples, but was reduced in the reactor at 350 °C for 1 hour. Following heat treatment, catalyst samples were tested in competitive acetylene hydrogenation reaction. For competitive hydrogenation experiments, the hydrocarbon feed gas comprised of 0.5 % acetylene and 35 % ethylene (balance nitrogen) was used at a flow rate of 70 ml/min. UHP hydrogen was fed into the reactor at a flow rate of 1.4 ml/min, giving a ratio of acetylene to ethylene to hydrogen of 1 : 70 : 4, respectively, and a space time of approximately 21,000 ml $g_{cat}^{-1}$ $hr^{-1}$. The acetylene to hydrogen ratio was chosen to be between that commonly used in industrial front-end and tail-end reactors, as was the ratio of acetylene to ethylene.[35] Feed gas flows were controlled with MKS mass flow controllers. Feed gas was initially channeled through a bypass line to establish a compositional baseline measurement before flowing through the catalyst beds. Gas composition was monitored with a Varian 3800 GC equipped with an FID detector. A 25-meter Varian capillary column was used. Temperature and gas flows were stabilized for 10 minutes prior to analyzing effluent compositions. Acetylene conversion and ethylene selectivity were calculated through Equations (1) and (2), respectively, for competitive hydrogenation data:

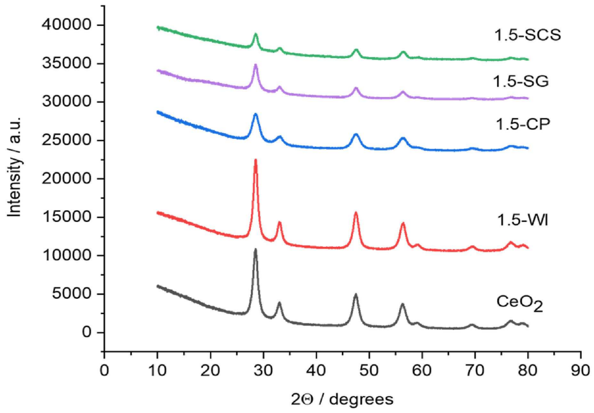

**Figure 1.** XRD patterns of $CeO_2$ and 1.5 wt % Ni–$CeO_2$ samples. All peaks shown belong to the $CeO_2$ fluorite crystal structure. No NiO peaks were detected.

$$\mathit{Acetylene\ Conversion} = \left[\frac{C_2H_{2\ in} - C_2H_{2\ out}}{C_2H_{2\ in}}\right] x\ 100 \tag{1}$$

$$\mathit{Ethylene\ Selectivity} = \left[1 - \frac{C_2H_{6\ out}}{C_2H_{2\ in} - C_2H_{2\ out}}\right] x\ 100 \tag{2}$$

There are two notes to make regarding the above selectivity equation. First, changes in ethylene concentration during the competitive hydrogenation (excess ethylene in the feed) are difficult to quantify accurately, hence the amount of ethane produced is used to infer selectivity. Second, selectivity may be negative, which indicates that some ethylene within the feed gas was over-hydrogenated to ethane. This equation is based on the area of the hydrocarbon peaks detected via the FID detector. This method of analysis does not accurately account for the deposition of carbon (oligomer formation) on the catalyst during reaction due to the low concentrations of acetylene used during competitive hydrogenation.

To quantify carbon deposition and catalyst stability, isothermal hydrogenation reactions were performed at 75 °C using

18673899, 2019, 5, Downloaded from https://chemistry-europe.onlinelibrary.wiley.com/doi/10.1002/cctc.201801976 by Purdue University (West Lafayette), Wiley Online Library on [11/07/2023]. See the Terms and Conditions (https://onlinelibrary.wiley.com/terms-and-conditions) on Wiley Online Library for rules of use; OA articles are governed by the applicable Creative Commons License

acetylene as the sole hydrocarbon feed gas. Select samples were loaded in varying amounts into reactors and heat treated as previously discussed. A feed gas mixture of UHP hydrogen (1 ml/min), acetylene (0.25 ml/min), and nitrogen (49.75 ml/min) was used, keeping the ratio of hydrogen to acetylene the same as for competitive hydrogenation. A bypass line was again used to quantify the amount of acetylene entering the system. During reaction, carbon deposition was quantified via GC measurement by taking the difference between the quantity of acetylene entering the reactor and the sum of acetylene, ethylene, and ethane exiting the reactor. No higher molecular weight volatile hydrocarbons were detected by the GC. Thus, the difference in carbon is herein referred to as oligomers. Ethylene, ethane, and oligomer selectivities were calculated through the following equations during these reactions [Eqs. (3)–(5)]. Trends in carbon deposition were verified through the carbon analysis previously discussed. This analysis was performed on select samples prior to reaction, after 3 hours on stream, and after 6 hours on stream.

$$Ethylene\ Selectivity = \left[\frac{C_2H_{4\ out}}{C_2H_{2\ in} - C_2H_{2\ out}}\right] x\ 100 \quad (3)$$

$$Ethane\ Selectivity = \left[\frac{C_2H_{6\ out}}{C_2H_{2\ in} - C_2H_{2\ out}}\right] x\ 100 \quad (4)$$

$$Oligomer\ Selectivity = \left[\frac{C_2H_{2\ in} - [C_2H_{2\ out} + C_2H_{4\ out} + C_2H_{6\ out}]}{C_2H_{2\ in} - C_2H_{2\ out}}\right] x\ 100 \quad (5)$$

To understand the formation of Ni clusters on ceria surfaces, we performed DFT calculations. All calculations were performed within spin-polarized density functional theory as implemented in Vienna Ab Initio Simulation Package (VASP).[36,37] The exchange-correlation potential was treated by the Perdew-Burke-Ernzerhof (PBE) gradient-corrected approximation.[38] The core electrons were described by projector augmented-wave (PAW)[39] method and the valance electronic wave functions were expanded in plane waves up to a cutoff energy of 400 eV. In order to properly describe the behavior of Ce *f* electrons, the DFT+*U* method with an effective $U=4.5$ eV is used.[40,41] The ceria surface is modeled using the $CeO_2(111)$ facet, because it has the lowest surface energy. The catalyst was modeled by *p* (3×3) nine-atomic-layer supercells with the bottom three layers fixed. A 1×1×1 Monkhorst-Pack mesh[42] *k*-point was used to sample the Brillouin zone. The convergence of relaxation was checked with the 0.05 eV/Å criterion and the total energy difference is less than $10^{-4}$ eV. The adsorption energy of a Ni atom was computed as follows: $E_{ads}=E(Ni_1+surface)-E(Ni_1)-E$ (free surface), where $E(Ni_1+surface)$, $E(Ni_1)$ and $E$(free surface) represent the calculated energies of the $CeO_2(111)$ supported Ni atom, the $Ni_1$ atom, and the $CeO_2(111)$ surface, respectively.

To understand the energy release for attaching a single $Ni_1$ atom at the most stable oxygen hollow site on the $CeO_2(111)$ surface towards $Ni_n$ ($n=10$, 15 and 20) cluster to form $Ni_{n+1}$ cluster on the ceria surface, the attachment energy ($E_{attach}$) is defined as follows [Eq. (6)]:

$$E_{attach} = E(Ni_{n+1}/CeO_2) + E(CeO_2) - E(Ni_n/CeO_2) - E(Ni_1/CeO_2) \quad (6)$$

where $E(Ni_n/CeO_2)$ and $E(Ni_1/CeO_2)$ represent the calculated energies of the $CeO_2(111)$ supported $Ni_n$ clusters and $Ni_1$ atom, respectively. The stable structures of the isolated Ni clusters are determined in previous reports.[43–45]

## Results

EPMA, BET, and XRD results for the bulk composition of calcined ceria and nickel-doped ceria samples are listed in Table 1. Actual nickel concentrations are near the target value of 1.5 wt%. BET analysis showed that samples had similar surface areas for coprecipitation and incipient wetness impregnation synthesis techniques. However, solution combustion synthesis produced samples of significantly lower surface area, and sol-gel synthesis produced samples of much higher surface area. Figure 1 shows XRD patterns for the $CeO_2$ and 1.5 wt% Ni–$CeO_2$ samples. As shown, no NiO phase was detected in these samples. Only peaks corresponding to the fluorite structure of Cerianite exist. Select samples were spiked with a Corundum standard and reanalyzed to refine lattice parameters. These values (Table 1) show that $CeO_2$ lattice parameter decreases with nickel incorporation because of the smaller ionic radius of nickel compared to cerium. These trends continued when sol-gel and wet impregnation samples with higher nickel loadings were analyzed (Table SI). A highly loaded sol-gel sample showed similar lattice parameter decrease, while that of a highly loaded wet impregnation sample remained similar to $CeO_2$.

Figure 2 shows HRTEM images of the 1.5-WI, 1.5-CP, and 1.5-SG samples with exposed $CeO_2$ planes indexed. No particles with lattice planes corresponding to NiO were found. 1.5-SCS is shown to have regions of highly agglomerated particles (Figure S1), which likely contribute to the lower surface area of this sample.

Competitive acetylene hydrogenation performance (using 70:1 mixture of ethylene to acetylene) is presented in Figure 3. 30 mg of Lindlar catalyst and 200 mg of all other samples were used. The Lindlar palladium catalyst is clearly more active than the nickel-ceria samples, with the 1.5-WI sample being the second most active catalyst. However, Lindlar and 1.5-WI

**Table 1.** EPMA composition, BET specific surface area, and XRD crystal size and lattice parameters of as-prepared ceria and nickel-doped ceria samples.

| Sample | Nickel composition [wt%] | Specific surface area [m²/g] | $CeO_2$ crystal size [nm] | $CeO_2$ lattice parameter [Å] |
|---|---|---|---|---|
| $CeO_2$ | – | 87.7 | 8.1 | 5.4127 |
| 1.5-CP | 1.54 | 81.4 | 5.0 | 5.4096 |
| 1.5-SG | 1.42 | 147.7 | 7.4 | 5.4060 |
| 1.5-SCS | 1.48 | 44.0 | 7.7 | 5.4090 |

© 2019 Wiley-VCH Verlag GmbH & Co. KGaA, Weinheim

18673899, 2019, 5, Downloaded from https://chemistry-europe.onlinelibrary.wiley.com/doi/10.1002/cctc.201801976 by Purdue University (West Lafayette), Wiley Online Library on [11/07/2023]. See the Terms and Conditions (https://onlinelibrary.wiley.com/terms-and-conditions) on Wiley Online Library for rules of use; OA articles are governed by the applicable Creative Commons License

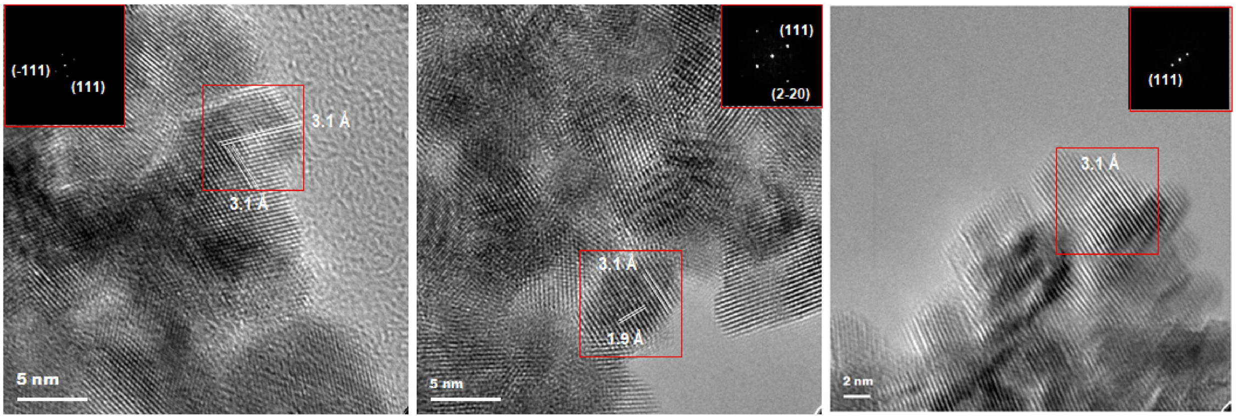

**Figure 2.** HRTEM images of as prepared 1.5-WI (left), 1.5-CP (middle), and 1.5-SG (right) samples. All indexed planes correspond to the $CeO_2$ crystal lattice, with interplanar spacings close to theoretical values. No NiO crystalline phases were found in these samples.

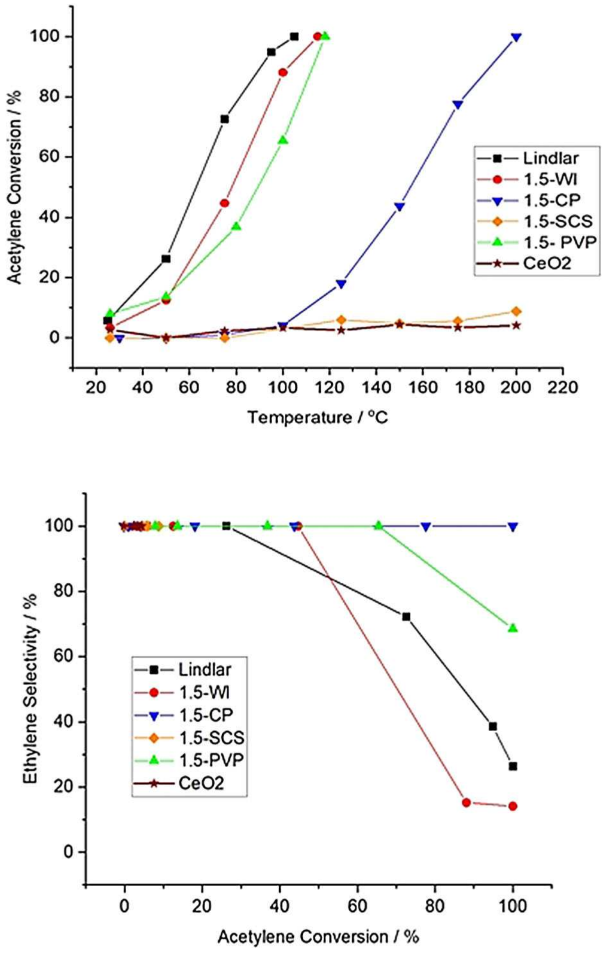

**Figure 3.** Competitive hydrogenation performance shown as light-off curves (top) and ethylene selectivity as a function of acetylene conversion (bottom).

samples produced large amounts of ethane at high acetylene conversions. The 1.5-SG sample did not produce ethane until 100% conversion was achieved. Remarkably, the 1.5-CP sample achieved 100% conversion without over-hydrogenating ethylene. While the 1.5-SCS and $CeO_2$ samples also did not produce ethane, their activities were quite low due to the lack of active sites in $CeO_2$ and the low surface area of 1.5-SCS. These results demonstrate that, under industrially relevant conditions of excess ethylene feed gas, ceria with incorporated nickel dopant atoms is both active in converting acetylene and can prevent over-hydrogenation of ethylene to ethane.

XPS analysis was used to investigate the difference in nickel surface species that leads to significantly lower ethylene selectivity in 1.5-WI versus 1.5-CP samples. It was believed that a surface enrichment of nickel species in 1.5-WI leads to metallic nickel clusters during the pre-reaction reduction. XPS spectra (Figure 4) were collected on these samples after reaction. NiO and metallic nickel ($Ni^0$) spectra were recorded for comparison. The locations of $Ni^0$ and NiO peaks are marked at 852.6 and 853.7 eV, respectively. These values agree with those reported in previous nickel XPS studies.[46,47] The main peak in the XPS spectra of 1.5-CP is marked at 855.1 eV, which Davidson et al. attribute to nickel incorporated into the ceria crystal lattice as a

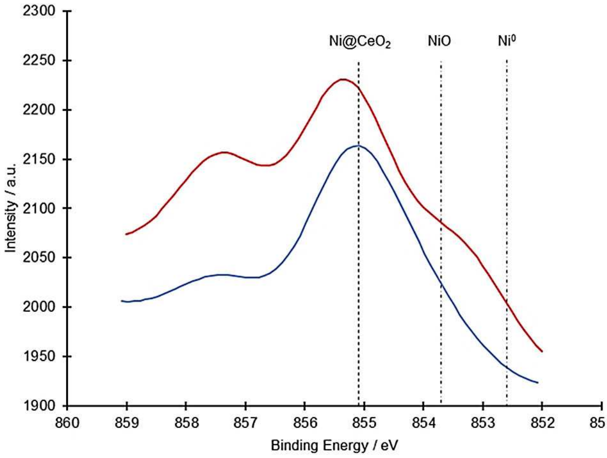

**Figure 4.** XPS spectra of 1.5-CP and 1.5-WI samples after reaction. The peak position of metallic nickel and nickel oxide standards are marked, as well as that of nickel doped into ceria.

© 2019 Wiley-VCH Verlag GmbH & Co. KGaA, Weinheim

18673899, 2019, 5, Downloaded from https://chemistry-europe.onlinelibrary.wiley.com/doi/10.1002/cctc.201801976 by Purdue University (West Lafayette), Wiley Online Library on [11/07/2023]. See the Terms and Conditions (https://onlinelibrary.wiley.com/terms-and-conditions) on Wiley Online Library for rules of use; OA articles are governed by the applicable Creative Commons License

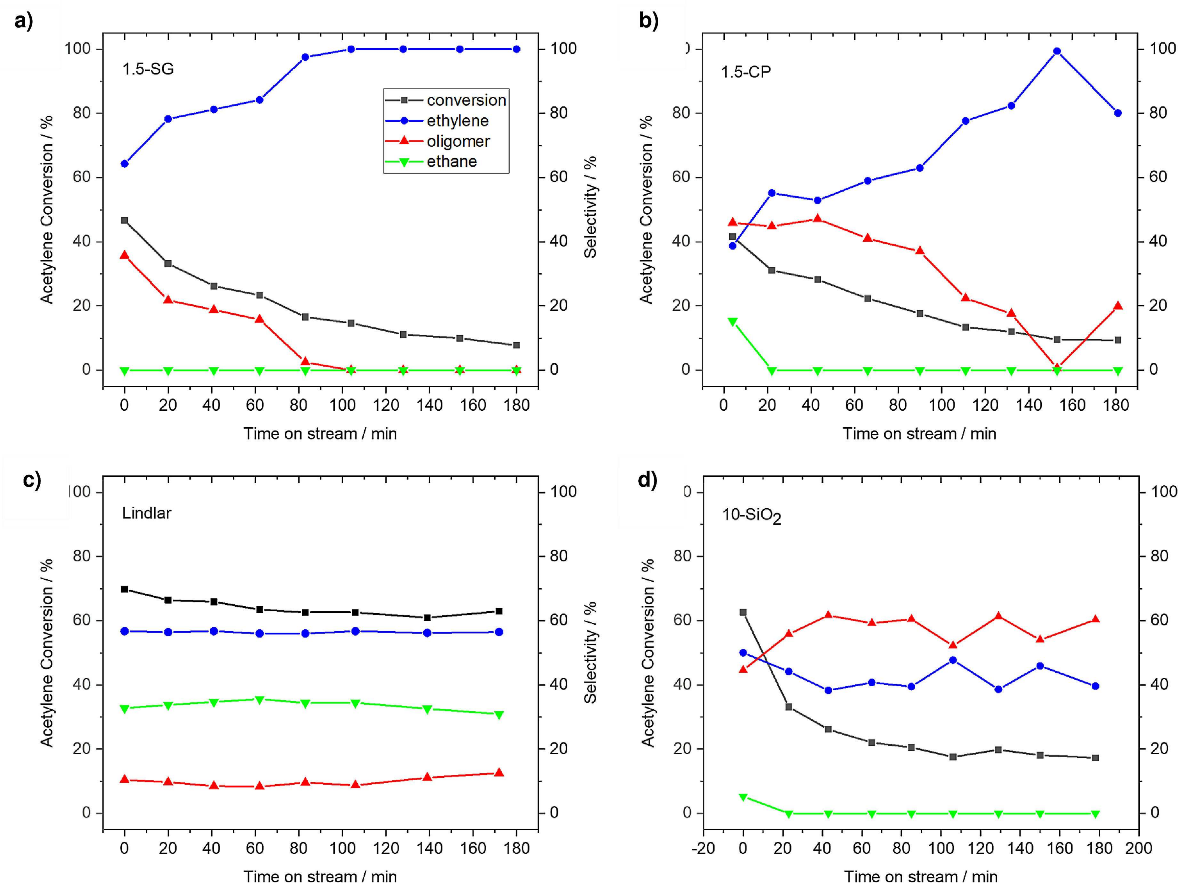

**Figure 5.** Isothermal hydrogenation test (T = 75 °C) results for 1.5-SG (150 mg) (a), 1.5-CP (380 mg) (b), Lindlar (15 mg) (c), and 10-$SiO_2$ (225 mg) (d) using acetylene as the sole hydrocarbon feed gas.

mixed oxide (Ni@$CeO_2$).[47] Their work shows that the binding energy of this peak varies from 855.5 to 855.0 eV depending on calcination temperature. Thus, both 1.5-WI and 1.5-CP contain Ni species in solid solution with $CeO_2$ after reaction. Both the 1.5-WI and 1.5-CP spent samples show a smaller peak at 857.4 eV. In previous work, this peak has been assigned to $Ni^{3+}$ and/or $Ni(OH)_2$ species.[47] The samples used in this work are not expected to contain the hydroxide, since they are all calcined at elevated temperatures, hence we have assigned this peak to the Ni solid solution in ceria. As shown, there is a lower energy shoulder present in the spent 1.5-WI sample that is absent in the spent 1.5-CP sample. The binding energy of this shoulder falls between that of $Ni^0$ and NiO peaks and indicates the formation of metallic nickel and/or nickel oxide ensembles on the ceria surface. This feature is clearly visible for a highly loaded 5.8 wt% Ni–$CeO_2$ wet impregnation sample (5.8-WI), shown in Figure S2. The absence of this feature in the spent 1.5-CP sample and an as-prepared 8.0-SG sample (Figure S2) demonstrates that the coprecipitation and sol gel synthesis techniques more thoroughly incorporate nickel ions into the ceria lattice. EDS mapping (Figure S3) and XPS measurement of $Ce^{3+}$ concentration (Table SII) corroborate both the dispersion and the incorporation of nickel into ceria for sol-gel samples. At 1.5 wt% loading, these ionic nickel species are retained even after reaction in a reducing environment. Incipient wetness impregnation of nickel nitrate solution onto pre-calcined ceria, on the other hand, did not fully incorporate nickel into the ceria lattice, which explains the reduced ethylene selectivity of this sample.

In addition to ethane production, oligomer formation also influences catalyst selectivity and stability. Isothermal testing using acetylene as the sole hydrocarbon feed gas was conducted on 1.5-SG (150 mg), 1.5-CP (380 mg), 10-$SiO_2$ (225 mg), and Lindlar (15 mg) samples to measure oligomer formation. Conversion and selectivity values were recorded for 3 hours TOS (time on stream). As shown in Figure 5, the Lindlar catalyst is the most stable catalyst in terms of conversion and product selectivity. However, ethylene selectivity remained below 60%, with ethane selectivity near 30% and oligomer selectivity near 10%. 10-$SiO_2$, which contained nickel nanoparticles (confirmed through XRD and TEM characterization of a 1.5-$SiO_2$ sample in Figure S4), shows signs of deactivation, with a noticeable drop in conversion over 3 hours TOS. This sample showed high oligomer selectivity (approximately 40–50%), which agrees with the findings of Trimm et al. In their work, Trimm et al. show that a 2 wt% Ni–$SiO_2$ sample had the same range in selectivity toward higher order hydrocarbon products.[8] Both 1.5-CP and 1.5-SG samples showed higher ethylene

© 2019 Wiley-VCH Verlag GmbH & Co. KGaA, Weinheim

18673899, 2019, 5, Downloaded from https://chemistry-europe.onlinelibrary.wiley.com/doi/10.1002/cctc.201801976 by Purdue University (West Lafayette), Wiley Online Library on [11/07/2023]. See the Terms and Conditions (https://onlinelibrary.wiley.com/terms-and-conditions) on Wiley Online Library for rules of use; OA articles are governed by the applicable Creative Commons License

selectivity than the palladium-based Lindlar catalyst and the 10-$SiO_2$ metallic nickel nanoparticle catalyst. In fact, 1.5-SG achieves 100% selectivity when accounting for both ethane and oligomer formation. Onda et al. show improved ethylene selectivity by doping nickel with tin. Yet, the highest ethylene selectivity achieved was only near 70% with higher order hydrocarbon selectivity ranging from approximately 30–50%.[12] Spanjers et al. found significantly improved ethylene selectivity in nickel-zinc alloys compared to unalloyed nickel, but the highest selectivity achieved by the alloy was only approximately 55%.[13] Ni-doped ceria demonstrates higher selectivity than these bimetallic samples.

Carbon compositional analysis was conducted on 1.5-SG and Lindlar samples after 0, 3, and 6 hours TOS to verify oligomer formation trends in the isothermal testing data. Since both samples had small amounts of carbon from air exposure prior to testing, the carbon content from 0 hours TOS (as prepared samples) was subtracted from carbon values obtained in samples after 3 and 6 hours on stream. Figure S5 shows the amount of deposited carbon during reaction and confirms the oligomer selectivity results. 1.5-SG, which produced no oligomers after 2 hours TOS, shows no increase in deposited carbon from 3 to 6 hours TOS. On the other hand, the Lindlar catalyst steadily produced oligomers throughout testing and shows a linear increase in deposited carbon content. These results demonstrate that doped nickel becomes selective for acetylene hydrogenation by nearly eliminating ethane production and mitigating oligomer formation.

Since metallic species are known to be responsible for hydrogenation reactions,[48] it is surprising to see oxidized Ni carrying out acetylene hydrogenation. However, multiple studies have used nickel (II) species to homogeneously catalyze hydrogenation reactions. Examples include nickel (II) phosphane for 1-octene hydrogenation to octane[49] and nickel boride for hydrogenation of nitrobenzene.[50] The presence of nickel is shown to improve redox properties and facilitate ceria reduction with resultant hydroxyl formation.[25] Having active sites on the ceria surface, without the presence of nickel, could also explain the formation of carbon deposits on ceria alone.

To investigate the selective hydrogenation of acetylene on Ni-doped ceria, we performed DFT computations to determine the mechanism in a separate study.[5] We found that oxygen vacancies on ceria surfaces are responsible for the hydrogenation activity of the doped ceria, and the role of Ni is to enhance the concentration of oxygen vacancies. Mechanistically, the catalysis is initiated by heterolytic dissociation of $H_2$, forming O–H and Ce–H species. This is followed by the adsorption and stepwise hydrogenation of acetylene. This mechanism, which is similar to those proposed by Huang et al.,[51] provides a much more plausible explanation of the efficient hydrogenation of alkynes than those proposed earlier.[52,53] Interestingly, for Ni-doped $CeO_2$, the adsorption state of an H atom on the Ni dopant is unstable since Ni is saturated in the square planar configuration. The avoidance of H adsorption prevents the reduction of $Ni^{2+}$ to $Ni^0$, which may otherwise agglomerate to form metallic Ni clusters on $CeO_2$.

The previous DFT calculations elucidated the catalytic mechanism for Ni-doped ceria in which the Ni dopant is incorporated into the ceria lattice.[5] As shown above, the coprecipitation and sol-gel synthesis samples are dominated by such structures. As a result, they possess the desired activity and selectivity for acetylene hydrogenation. However, the previous study[5] did not consider the situation in which $Ni^{2+}$ is deposited on ceria surfaces, which corresponds to the samples prepared via incipient wetness impregnation. To understand the loss of selectivity in the 1.5-WI sample at high temperatures, we have analyzed the energetics of Ni adsorption and cluster formation on $CeO_2(111)$ using DFT, as presented in the supporting information. It is plausible that the atomic Ni species are adsorbed on the surface of $CeO_2(111)$, rather than inside the lattice, in such samples. The adsorption energy of a $Ni_1$ single atom on $CeO_2(111)$ is calculated to be −3.24 eV, suggesting a strong interaction with the ceria surface. The binding energies for $Ni_n$ clusters on $CeO_2(111)$ are calculated to be −5.33~−5.71 eV (Table SIII), indicating that they are strongly bonded to ceria. Now, we consider the formation of a $Ni_{n+1}$ cluster ($n$ = 10, 15, and 20), shown in Figure S6. These calculations indicated that the energy release of −1.50~−2.03 eV for attaching a single $Ni_1$ atom from its most stable oxygen hollow site to the $Ni_n$ clusters on $CeO_2(111)$ is an exothermic process for $Ni_{n+1}$ clusters on $CeO_2(111)$. This suggests that Ni atoms can readily sinter to form clusters on the ceria support. These Ni clusters are known to catalyze the hydrogenation non-selectively, behaving similarly to the Lindlar catalyst.

## Conclusions

Nickel dopants were previously shown to increase the hydrogenation activity of ceria. This current work demonstrates that nickel dopants, acting as a ceria promoter, not only improve activity, but also facilitate selective hydrogenation. Coprecipitation and sol-gel synthesis techniques allowed for nickel to homogeneously dope into the ceria lattice. Ni-doped ceria completely converted acetylene while preventing over-hydrogenation and reducing oligomer formation. However, incipient wetness impregnation created nickel species on the ceria surface. DFT calculations show sintering of nickel surface species into metallic nickel nanoparticles to be favorable under reaction conditions. Metallic nickel oligomerizes hydrocarbon reactants, reducing ethylene selectivity. Selective acetylene hydrogenation performance is clearly linked to the type of nickel species within ceria catalysts. Thus, this reaction provides a sensitive probe of the extent to which nickel is incorporated into the ceria lattice.

## *Acknowledgements*

*This work is supported by U.S. Department of Energy grant DE-FG02-05ER15712 to AD. Additional funding for the computational studies was provided by the U.S. Air Force Office of Scientific Research (FA9550-18-1-0413 to HG), Foundation of Jiangxi Educa-*

© 2019 Wiley-VCH Verlag GmbH & Co. KGaA, Weinheim

18673899, 2019, 5, Downloaded from https://chemistry-europe.onlinelibrary.wiley.com/doi/10.1002/cctc.201801976 by Purdue University (West Lafayette), Wiley Online Library on [11/07/2023]. See the Terms and Conditions (https://onlinelibrary.wiley.com/terms-and-conditions) on Wiley Online Library for rules of use; OA articles are governed by the applicable Creative Commons License

*tional Committee, China (GJJ160884), and National Natural Science Foundation of China (21673040). SZ and SL also thank the China Scholarship Council (201608360178) and Fujian Province Scholarship Council, respectively, for supporting their visits to UNM. The calculations are performed at the National Energy Research Scientific Computing (NERSC) center.*

## *Conflict of Interest*

The authors declare no conflict of interest.

**Keywords:** Acetylene hydrogenation · catalyst synthesis · ceria · nickel · selective hydrogenation

[1] G. Vilé, S. Wrabetz, L. Floryan, M. E. Schuster, F. Girgsdies, D. Teschner, J. Pérez-Ramírez, *ChemCatChem* **2014**, *6*, 1928–1934.
[2] G. Vilé, D. Albani, N. Almora-Barrios, N. López, J. Pérez-Ramírez, *ChemCatChem* **2016**, *8*, 21–33.
[3] G. Vilé, S. Colussi, F. Krumeich, A. Trovarelli, J. Pérez-Ramírez, *Angew. Chem. Int. Ed.* **2014**, *53*, 12069–12072.
[4] G. Vilé, B. Bridier, J. Wichert, J. Pérez-Ramírez, *Angew. Chem. Int. Ed.* **2012**, *51*, 8620–8623.
[5] C. Riley, S. Zhou, D. Kunwar, A. De La Riva, E. Peterson, R. Payne, L. Gao, S. Lin, H. Guo, A. Datye, *J. Am. Chem. Soc.* **2018**, *140*, 12964–12973.
[6] M. Nolan, *J. Mater. Chem.* **2011**, *21*, 9160–9168.
[7] F. Studt, F. Abild-Pedersen, T. Bligaard, R. Sørensen, C. Christensen, J. Nørskov, *Science* **2008**, *320*, 1320–1322.
[8] D. L. Trimm, I. O. Y Liu, N. W. Cant, *J. Mol. Catal. A* **2008**, *288*, 63–74.
[9] D. L. Trimm, I. O. Y Liu, N. W. Cant, *Appl. Catal. A* **2010**, *374*, 58–64.
[10] D. L. Trimm, N. W. Cant, I. O. Y. Liu, *Catal. Today* **2011**, *178*, 181–186.
[11] J. C. Rodríguez, A. J. Marchi, A. Borgna, A. Monzón, *J. Catal.* **1997**, *171*, 268–278.
[12] A. Onda, T. Komatsu, T. Yashima, *Phys. Chem. Chem. Phys.* **2000**, *2*, 2999–3005.
[13] C. S. Spanjers, J. T. Held, M. J. Jones, D. D. Stanley, R. S. Sim, M. J. Janik, R. M. Rioux, *J. Catal.* **2014**, *316*, 164–173.
[14] A. Borodziński, *Catal. Lett.* **1999**, *63*, 35–42.
[15] G. X. Pei, X. Y. Liu, A. Wang, A. F. Lee, M. A. Isaacs, L. Li, X. Pan, X. Yang, X. Wang, Z. Tai, K. Wilson, T. Zhang, *ACS Catal.* **2015**, *5*, 3717–3725.
[16] J. Osswald, R. Giedigkeit, R. E. Jentoft, M. Armbrüster, F. Girgsdies, L. Kovnir, T. Ressler, Y. Grin, R. Schlögl, *J. Catal.* **2008**, *258*, 210–218.
[17] H. B. Liu, U. Pal, A. Medina, C. Maldonado, J. A. Ascencio, *Phys. Rev. B* **2005**, *71*, 075403.
[18] N. A. Khan, S. Shaikhutdinov, H. J. Freund, *Catal. Lett.* **2006**, *108*, 159–164.
[19] T. V. Choudhary, C. Sivadinarayana, A. K. Datye, D. Kumar, D. W. Goodman, *Catal. Lett.* **2003**, *86*, 1–8.
[20] J. B. Wang, Y. L. Tai, W. P. Dow, T. J. Huang, *Appl. Catal. A* **2001**, *218*, 69–79.
[21] O. A. Bereketidou, M. A. Goula, *Catal. Today* **2012**, *195*, 93–100.
[22] C. Tang, J. Li, X. Yao, J. Sun, Y. Cao, L. Zhang, F. Gao, Y. Deng, L. Dong, *Appl. Catal. A* **2015**, *494*, 77–86.
[23] J. Barrault, A. Alouche, V. Paul-Boncour, L. Hilaire, A. Percheron-Guegan, *Appl. Catal.* **1989**, *46*, 269–279.
[24] K. Shimura, K. Shimizu, *Green Chem.* **2012**, *14*, 2983–2985.
[25] C. Lamonier, A. Ponchel, A. D'Huysser, L. Jalowiecki-Duhamel, *Catal. Today* **1999**, *50*, 247–259.
[26] A. Ponchel, A. D'Huysser, C. Lamonier, L. Jalowiecki-Duhamel, *Phys. Chem. Chem. Phys.* **2000**, *2*, 303–312.
[27] L. Wang, S. Zhang, Y. Liu, *J. Rare Earths* **2008**, *26*, 66–70.
[28] S. Mahammadunnisa, P. Manoj Kumar Reddy, N. Lingaiah, C. Subrahmanyam, *Catal. Sci. Technol.* **2013**, *3*, 730–736.
[29] L. Jalowiecki-Duhamel, S. Debeusscher, H. Zarrou, A. D'Huysser, H. Jobic, E. Payen, *Catal. Today* **2008**, *138*, 266–271.
[30] G. Wrobel, C. Lamonier, A. Bennani, A. D'Huysser, A. Aboukaïs, *J. Chem. Soc. Faraday Trans.* **1996**, *92*, 2001–2009.
[31] K. Tang, W. Liu, J. Li, J. Guo, J. Zhang, S. Wang, S. Niu, Y. Yang, *ACS Appl. Mater. Interfaces* **2015**, *7*, 26839–26849.
[32] J. M. García-Vargas, J. L. Valverde, A. De Lucas-Consuegra, B. Gómez-Monedero, P. Sánchez, F. Dorado, *Appl. Catal. A* **2012**, *431–432*, 49–56.
[33] I. Pashalidis, C. R. Theocharis, *Charact. Porous Solids V* **2000**, *128*, 643–652.
[34] G. Pantaleo, V. La Parola, F. Deganello, R. K. Singha, R. Bal, A. M. Venezia, *Appl. Catal. B* **2016**, *189*, 233–241.
[35] A. J. McCue, J. A. Anderson, *Front. Chem.* **2015**, *9*, 142–153.
[36] G. Kresse, J. Furthmüller, *Comput. Mater. Sci.* **1996**, *6*, 15–50.
[37] G. Kresse, J. Furthmüller, *Phys. Rev. B* **1996**, *54*, 11169–11186.
[38] J. P. Perdew, K. Burke, M. Ernzerhof, *Phys. Rev. Lett.* **1996**, *77*, 3865–3868.
[39] P. E. Blöchl, *Phys. Rev. B* **1994**, *50*, 17953–17979.
[40] S. Fabris, G. Vicario, G. Balducci, S. De Gironcoli, S. Baroni, *J. Phys. Chem. B* **2005**, *109*, 22860–22867.
[41] M. D. Krcha, M. J. Janik, *Int. J. Quantum Chem.* **2014**, *114*, 8–13.
[42] H. Monkhorst, J. Pack, *Phys. Rev. B* **1976**, *13*, 5188–5192.
[43] K. R. Hahn, A. P. Seitsonen, M. Iannuzzi, J. Hutter, *ChemCatChem* **2015**, *7*, 625–634.
[44] Q. Wang, K. H. Lim, S. W. Yang, Y. Yang, Y. Chen, *Theor. Chem. Acc.* **2011**, *128*, 17–24 (2011).
[45] S. K. Nayak, S. N. Khanna, B. K. Rao, P. Jena, *J. Phys. Chem. A* **1997**, *101*, 1072–1080.
[46] A. P. Grosvenor, M. C. Biesinger, R. S. C. Smart, N. S. McIntyre, *Surf. Sci.* **2006**, *600*, 1771–1779.
[47] A. Davidson, J. F. Tempere, M. Che, H. Roulet, G. Dufour, *J. Phys. Chem.* **1996**, *100*, 4919–4929.
[48] G. C. Bond, *Metal-Catalysed Reactions of Hydrocarbons.* (Springer, 2005).
[49] I. M. Angulo, A. M. Kluwer, E. Bouwman, *Chem. Commun.* **1998**, 2689–2690 (1998).
[50] D. J. Collins, A. D. Smith, B. H. Davis, *Ind. Eng. Chem. Prod. Res. Dev.* **1982**, *21*, 279–281.
[51] Z. Q. Huang, L. P. Liu, S. Qi, S. Zhang, Y. Qu, C. R. Chang, *ACS Catal.* **2018**, *8*, 546–554.
[52] J. Carrasco, G. Vilé, D. Fernández-Torre, R. Pérez, J. Pérez-Ramírez, M. V. Ganduglia-Pirovano, *J. Phys. Chem. C* **2014**, *118*, 5352–5360.
[53] M. García-Melchor, L. Bellarosa, N. López, *ACS Catal.* **2014**, *4*, 4015–4020.

Manuscript received: December 5, 2018
Revised manuscript received: January 13, 2019
Accepted manuscript online: January 15, 2019
Version of record online: February 14, 2019

© 2019 Wiley-VCH Verlag GmbH & Co. KGaA, Weinheim

18673899, 2019, 5, Downloaded from https://chemistry-europe.onlinelibrary.wiley.com/doi/10.1002/cctc.201801976 by Purdue University (West Lafayette), Wiley Online Library on [11/07/2023]. See the Terms and Conditions (https://onlinelibrary.wiley.com/terms-and-conditions) on Wiley Online Library for rules of use; OA articles are governed by the applicable Creative Commons License